A short review on diffusion coefficients in magnesium alloys and related applications

Shi, Hui; Huang, Yuanding; Luo, Qun; Gavras, Sarkis; Willumeit-Römer, Regine; Hort, Norbert

Published in:
Journal of Magnesium and Alloys

DOI:
10.1016/j.jma.2022.12.003

Publication date:
2022

Document Version
Publisher's PDF, also known as Version of record

Available online at www.sciencedirect.com

ScienceDirect

Journal of Magnesium and Alloys 10 (2022) 3289–3305

www.elsevier.com/locate/jma

Review

A short review on diffusion coefficients in magnesium alloys and related applications

Hui Shi[a], Yuanding Huang[a,*], Qun Luo[b,*], Sarkis Gavras[a], Regine Willumeit-Römer[a], Norbert Hort[a,c]

[a] *Institute of Metallic Biomaterials, Helmholtz-Zentrum Hereon, Max-Planck-Str.1, Geesthacht 21502, Germany*

[b] *State Key Laboratory of Advanced Special Steels and Shanghai Key Laboratory of Advanced Ferrometallurgy, School of Materials Science and Engineering, Shanghai University, Shanghai 200444, China*

[c] *Institute of Product and Process Innovation, Leuphana University Lüneburg, Universitätsallee 1, Lüneburg D-21335, Germany*

Received 22 August 2022; received in revised form 2 December 2022; accepted 6 December 2022
Available online 16 December 2022

Abstract

To have a better understand on the change of microstructure via kinetics, the diffusion behavior of Mg alloys is of special interest to researchers. Meanwhile, diffusion coefficients of Mg based alloys can explain and represent their diffusion behavior well. The evolution of experimental and calculated methods for detecting and extracting diffusion coefficients was discussed briefly. The reasonable diffusion data, especially self-diffusion coefficients, impurity diffusion coefficients and inter-diffusion coefficients of Mg alloys, were reviewed in detail serving to design the Mg alloys with higher accuracy. Then the practical applications of diffusion coefficients of Mg alloys were summarized, including diffusional mobility establishing, precipitation simulation and mechanical properties prediction.

Keywords: Magnesium alloys; Diffusion coefficients; Atomic mobility; Precipitation; Mechanical properties.

1. Introduction

Magnesium-based alloys have been the recent research focus in fields such as automotive, aerospace and 3C industries owing to their high specific strength, low density, good castability and other potential performance [1–7]. However, there still exist several limitations [8–10] restricting their practical applications, e.g. poor corrosion resistance, low creep resistance and limited room temperature deformability. In order to improve the comprehensive performance of Mg-based alloys, alloying and heat treatment were normally utilized for regulating their microstructures, which are strongly influenced by their diffusion behavior [7,11–15]. Generally, the diffusion behavior of Mg alloys is reflected as diffusion coefficients in Mg-based alloys.

Self-diffusion coefficients, impurity diffusion coefficients and inter-diffusion coefficients are mainly reported [16–18] to indicate diffusion behavior for Mg alloys. When all the atoms exchanging positions are of the same type, diffusion coefficient of these atoms in pure metals is termed as self-diffusion coefficient. The impurity diffusion coefficient of a solute atom in pure metal can be measured at extremely low concentration of solute atoms. A different type of diffusion coefficient compared to these two types of diffusion coefficients is inter-diffusion coefficient $\tilde{D}$ that occurs between two metals depends on chemical concentration gradient. The inter-diffusion coefficient can reflect diffusion behavior adequately for some practical applications [19]. By now, much efforts including diffusion couple and calculated methods has been expended on investigating diffusivities data for binary Mg alloys [16].

* Corresponding authors.
E-mail addresses: Yuanding.Huang@hereon.de (Y. Huang), qunluo@shu.edu.cn (Q. Luo).

https://doi.org/10.1016/j.jma.2022.12.003

These various diffusion coefficients are also the bases of the diffusion mobility database. In the past decades, the CALPHAD (CALculation of PHAse Diagrams) technique embedding DICTRA (Diffusion Controlled TRAnsformation) module has developed as a computational tool to establish diffusional mobilities data [13,16,20–25] and predict phase equilibria. Compared to comprehensiveness in multicomponent thermodynamic database, the development of atomic mobility database is limited to binary Mg systems. The atomic mobilities database for few ternary systems, containing Mg–Al–Sn [21], Mg–Al–Zn [16,24], Mg–Al–Ga [20] and Mg–Al–Li [23], were developed, which hinder the precipitation simulation for multicomponent Mg alloys and following mechanical properties prediction. Therefore, studying on diffusion behavior is still an area of active present research [26], owing to the lack of diffusivities data for ternary or high-order magnesium alloys.

Experimental measurements and assistant calculation methods for determining relatively precise diffusion coefficients were reviewed in this paper. Main diffusion coefficients of Mg-based alloys shown in different literature were summarized, which provide the theoretical basis for promoting the atomic mobility database of binary and multi-component Mg alloys. The diffusion database of Mg alloys from the recent research has been applied to investigating their precipitating evolution [27,28] and predicting their diffusion controlled properties. For instance, yield strength and hardness for Mg alloys could be effectively estimated according to precipitation simulation. Creep behaviors of Mg alloys at elevated temperature [29] are also highly dependent on their diffusion data. Thus, Mg alloys with high performance are expected to be designed with reference to the review of these works.

2. Development of methods for determining diffusion coefficients of Mg alloys

2.1. Experimental methods

It is well known that diffusion coefficient data are the foundation for constructing mobility database of Mg alloys, while there is still a lack of sufficient experimental diffusion data. Pure Mg is prone to oxide and evaporate at high temperatures [30–32], which brings some obstacles to diffusion experiments. In addition, the diffusion occurring between pure Mg and other elements or between two different Mg-based alloys requires a considerable amount of time to complete the whole diffusion process at lower temperatures. That is, the diffusion experiments at low temperatures also show some shortcomings, which can be easily understood based on the fundamental diffusion mechanism and theory [19,33]. Therefore, various experimental methods have been performed in Mg alloys to avoid tough and time-consuming processes as mentioned above.

Most self-diffusion coefficients and impurity coefficients of Mg alloys were measured from the 1950s to the 1990s using the reliable tracer method [34–38], which usually utilized deposited isotopes attached on the surface of pure Mg to detect diffusion profiles. However in addition to this being a laborious and costly method, it is difficult to find suitable radioactive isotopes for some common elements such as Li, Ca and Al, which further restricts the widespread use of tracer experiments. Although the impurity diffusion coefficient of Al in Mg [39] and Mg self-diffusion [40] were measured by a similar method, secondary ion mass spectroscopy (SIMS), sputter-roughening induced the uncertainty of experimental results. Recently, Yang et al. [41] prepared the semi-infinite diffusion and characterized the samples through Glow Discharge Optical Emission Spectroscopy (GD-OES) technique, which reduced the error caused by SIMS to some extent.

The common experimental method used nowadays is diffusion couple [21,42] for detecting diffusion coefficients. The diffusion couples suitable for Mg alloys can roughly be divided into solid-state diffusion couples and liquid-solid diffusion couples. Solid-solid diffusion couples for binary Mg-based alloys usually consist of pure elements [15,43–65]. Their annealing temperatures must be lower than the eutectic temperatures to avoid the formation of liquid phases. This method can also be extrapolated to detect the diffusion coefficients of Mg-based multi-component systems in a single sample [21–23,25,66–68]. However, some pure elements are easy to oxidize and cannot be easily prepared as pure diffusion samples, for example, certain rare earth elements and Ca. Therefore, Mg-rich binary alloys can replace these pure elements as the components of solid-solid diffusion couples. Furthermore, liquid-solid diffusion couple (LSDC) method was conducted to measure the diffusion coefficients of Mg alloys. The dip method was carried out for Mg alloys by Zhang et al. [69] and Dai et al. [70] based on the idea of solid-liquid contact. Nevertheless, the liquid part has a tendency to oxidize, and then the dense oxide film on the surface of the liquid part hinders the diffusion between materials. Thus, Zhao et al. [26,71–73] firstly proposed a novel and convenient liquid-solid diffusion couple method to obtain the diffusion coefficients in Mg alloys at the elevated temperatures above the eutectic temperatures. Choosing a suitable experimental method according to the specific Mg systems is one of the key point to get accurate diffusion datasets.

After yielding reliable experimental composition profiles, the diffusion coefficients are extracted using a modified equation based on Fick's law. Boltzmann–Matano analysis [74] is a common method for extracting concentration-dependent inter-diffusion coefficients, while some errors are caused due to the difficulty in evaluating the concentration gradients near phase boundary areas [22,75] and determining the Matano plane location. Several other methods, Sauer–Freise method [76], Hall method [77], and Wagner method [78] are developed to eliminate these errors. Sauer and Freise [76] defined a new equation for avoiding calculating the position of the Matano plane. However, this method is still closely associated with the concentration gradients, which are inaccurate at the end of composition profiles. Hall [77] conducted a further modification based on the Boltzmann–Matano strategy, analyzing the end of composition profiles with a linear fit. This method alleviates the aforementioned two problems, and

serves as the main way to extract the diffusion coefficients from experimental results. Additionally, the Hall method indeed does well when calculating the diffusion coefficients at the first and last 10% composition range [79], especially when evaluating the impurity coefficients. Therefore, the selection of these modified methods should rely on the composition range. However, it is apparent that the Hall method is only valid when the diffusion coefficients are constant or nearly constant at the low composition regions [79], indicating that certain conditions are required to use this technique. The Wagner method [78] uses a similar equation as the Sauer–Freise method, which can also extract inter-diffusion coefficients reliably on the basis of accurate concentration gradient data.

Apart from these traditional methods, the optimized numerical inverse method is implemented to exact diffusion coefficients from experimental composition profiles. Zhang and Zhao [75] developed a MatLab code by using Forward-simulation analysis (FSA) analysis, showing good self-consistency for calculating diffusion coefficients. FSA method is a numerical inverse method, which evaluates the diffusion coefficients directly from diffusion composition profiles. To accelerate the speed of the program, the diffusion coefficients calculated by traditional methods are used as initial parameters. FSA method would also obtain the diffusion coefficients with random starting values. The agreement between results extracted by FSA method and traditional methods demonstrates the reliability of FSA.

2.2. First-principle methodology

Diffusion coefficients in stable phases have been studied experimentally, which only concentrated on partial Mg binary systems and few Mg ternary systems. Additionally, there still exists some difficulty in measuring diffusion coefficients over the whole temperature range. The diffusion data in metastable phases cannot be extracted using experimental methods and analysis strategies. Therefore, density functional theory (DFT) method is adjusted based on accurate experimental data, and then applied to predict diffusion coefficients of unexamined Mg systems.

The DFT calculations are generally performed by Vienna ab initio simulation package (VASP), a plane-wave basis set [80]. It is easy to find that the self-diffusion and impurity diffusion coefficients in Mg vary with different DFT settings. Different choices for diffusion model, energetic, entropic and attempt frequency calculations could lead to different DFT data. Exchange correlation (XC) functional [81] of local density approximation (LDA), the generalized gradient approximation (GGA) [82], ultra-soft pseudopotential (USPP) and projector augmented wave (PAW) are commonly used in evaluating diffusivities of Mg alloys [83,84], while PAW was confirmed to be a relatively reasonable way. The vacancy concentration, solute-vacancy exchange jump frequencies and the correlation factors can determine the values of not only self and impurity diffusivities, but also inter-diffusion coefficients [83]. Vacancy concentration can be obtained using the supercell method [85]. Jump frequencies are calculated using a quasi-harmonic Debye model [86,87]. The correlation factors of solute diffusion in hexagonal closed pack (hcp) lattice can be assessed using 8-frequency model and the 13-frequency model [88,89]. Supercell size convergence test, K-point convergence test, thermodynamic properties of pure hcp Mg, and vacancy formation in pure hcp Mg should be adjusted constantly to meet the calculated requirements. All the experimental and calculation diffusivities data were fitted using Arrhenius equation as following:

$$D = D_0 exp\left(-\frac{Q_d}{RT}\right) \tag{1}$$

Where R is the gas constant, T is the absolute temperature, D_0 and Q_d are the pre-exponential factor and activation energy for diffusion, respectively.

3. Diffusion coefficients of different elements in Mg systems

3.1. Self-diffusion coefficients of pure Mg

Shewmon and Rhines [34] firstly investigated the self-diffusion coefficients in Mg using the tracer method and proposed the hypothesis that an anisotropy of diffusion existed. This hypothesis was soon proven to be true in their later research [35], which was performed on oriented single crystal Mg. Differences in Mg self-diffusion coefficients parallel and perpendicular to the c-axis were also studied [40,90] using radioactive tracer and SIMS method, demonstrating good consistency with previous data [35] at a temperature range of 740–908 K. All the experimental results are plotted as different symbols in Fig. 1.

As polycrystalline Mg is more widely used compared with single crystal Mg, the average diffusion coefficients are introduced as the main parameters [91]. For hcp diffusivity, the total diffusivity can be expressed as follows:

$$D_{ave} = \frac{2}{3}D_{basal} + \frac{1}{3}D_{prism} \tag{2}$$

where D_{basal} and D_{prism} are the anisotropic diffusion coefficients along the basal plane and c-axis, respectively. The calculation results obtained from the DFT method [22,84,85,92–94] are presented as the average diffusion coefficients in Fig. 1. The deviation between experimental data and calculations at high temperatures can be attributed to the dominance of di-vacancies, which are not included in calculation process [95,96]. That is, two adjacent vacancies will be formed as a cluster, which is stable and accelerate the diffusion rate at elevated temperatures. The measured results and part of computed results in Fig. 1 were also assessed by Zhong and Zhao [16] using the above holistic approach, indicating that $D_{Mg}^{hcp\ Mg} = 2.9\times10^{-5}\ e^{-125748/RT}$ (m^2/s). It is worth noting that self-diffusion coefficients in metastable fcc Mg phase were calculated by Zhong et al. [22] and Hooshmand et al. [84], which provides comprehensive diffusivity for evaluating the mobility database. The calculated Arrhenius equation of

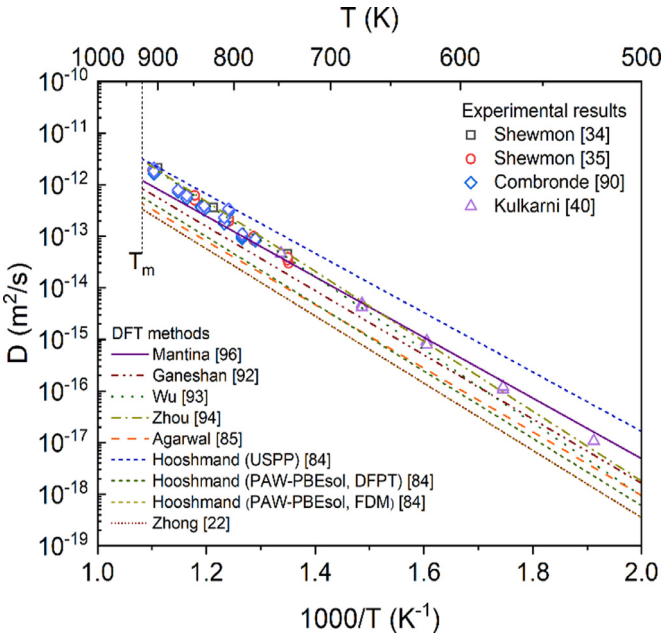

Fig. 1. Summary of experimental and calculation studies on self-diffusion coefficients of hcp Mg [22,34,35,40,84,85,90,92–94,96].

the self-diffusion coefficients in fcc Mg phase is $D_{Mg}^{fcc\ Mg} = 1.5\times10^{-5}\ e^{-126000/RT}$ (m^2/s).

3.2. Impurity diffusion coefficients of alloying elements in Mg

3.2.1. Impurity diffusion coefficients of rare earth elements in Mg

Mg–RE systems have received great attention as RE elements are well known to improve the properties of Mg alloys at elevated temperatures. Different intermetallic compounds existing in Mg–RE alloys have been widely investigated using diffusion couples methods. However, few studies on the impurity diffusion coefficients of RE elements in Mg were performed. This paper provides a comparison between the experimental and first principles calculations data of the impurity diffusion coefficients of main addition RE elements (Y, Sc, Nd, La, Ce and Gd) in hcp Mg, as shown in Fig. 2.

Yttrium has a stable hcp crystal structure, and its self-diffusion coefficients along the c-axis and basal plane have been reported by Gornyj et al. [97]. The stable phases in Mg–Y systems were developed in literature [15,48,57], indicating that three types of intermetallic compounds $Mg_{24}Y_5$, Mg_2Y and MgY are formed in this system. Nevertheless, the impurity diffusivity of polycrystalline Y in Mg has just been revealed recently using the diffusion couple methods [15,57,73]. Fig. 2(a) presents the comparison between experimental and calculated impurity diffusivities [17,85,94] of Y in hcp Mg, which shows great consistency. Thus, the reliable impurity diffusion coefficients of Y in Mg can be evaluated as the average of experimental values. Additionally, compared with the self-diffusivity of Mg (Fig. 1), the impurity diffusivity of Y in Mg is approximately one order of magnitude lower. The similar phenomenon is also shown in Fig. 2(c), for neodymium. Many attempts have been made by Xu et al. [98] to determine the impurity diffusivity of Nd in liquid Mg, whose results were denoted using a blue open circle. Then Paliwal et al. [53] obtained the impurity diffusivity of Nd in a relatively narrow temperature range (40 K), which brought a large uncertainty when assessing the activation energy. Meanwhile, Zhong and Zhao [16] utilized the novel LSDC method to determine diffusivity at 888 and 903 K, presenting the same issue with the study of Paliwal et al. [53]. Even though experimental data in Xu et al. [98] are in good agreement with first principle calculations of impurity diffusivity of Nd in Mg, the diffusivity at low temperature cannot be extrapolated accurately using data measured at elevated temperatures. The impurity diffusivities of Nd, La, Ce and Gd in Mg reported in Wu et al. [93] varied greatly from other data in Fig. 2, as confirmed in their own work. Thus their work was also not considered when evaluating diffusivities of these four elements. Therefore, reasonable impurity diffusivities of Nd in Mg can be identified combining the experimental values with DFT data [83,85]. The impurity diffusivities of Sc, La, Ce and Gd in Mg have been investigated over a wide range of temperatures [26,43,57,99], which agree well with DFT values in Jhou et al. [17,83,85,94]. Y and Sc have lower impurity diffusivities than Mg self-diffusion coefficients. Furthermore, it can be easily concluded that the impurity diffusivities of Y and Sc in Mg are much lower than that of other RE elements (Fig. 2). That is, Y and Sc diffuse more slowly than other elements in Mg.

The impurity diffusivities of the aforementioned RE elements in Mg are all detected experimentally, and compared with DFT results comprehensively. However, the diffusion data of the rest RE elements are not determined using experimental methods. Firstly, it is quite difficult to prepare their diffusion couples or to search for suitable radioactive isotopes. Secondly, these elements are not widely used in Mg alloys. In spite of such situations, the diffusivities were still calculated using DFT methods [83,85,93]. The DFT data shows that heavy RE elements diffuse more slowly than light RE elements in hcp Mg, and light RE elements tend to diffuse faster than self-diffusion of Mg. In addition, the impurity diffusivities of these elements in Mg can be set as the average values of DFT data, which serve as the fundamental of mobility parameters.

3.2.2. Impurity diffusion coefficients of some common elements in Mg

The impurity diffusion coefficients of six alloying elements in Mg shown in Fig. 3 were investigated more widely than other elements, and the diffusion data of these Mg binary systems were applied to ternary systems in the Section 3.3. Seven sets of impurity diffusivities of Al in Mg were compared with calculation results, indicating that experimental data from [24,45,72] are well consistent with calculated data. However, this data was much lower than those diffusivities determined experimentally by Brennan et al. [39] using SIMS method, similar to the tracer method but not reliable. The

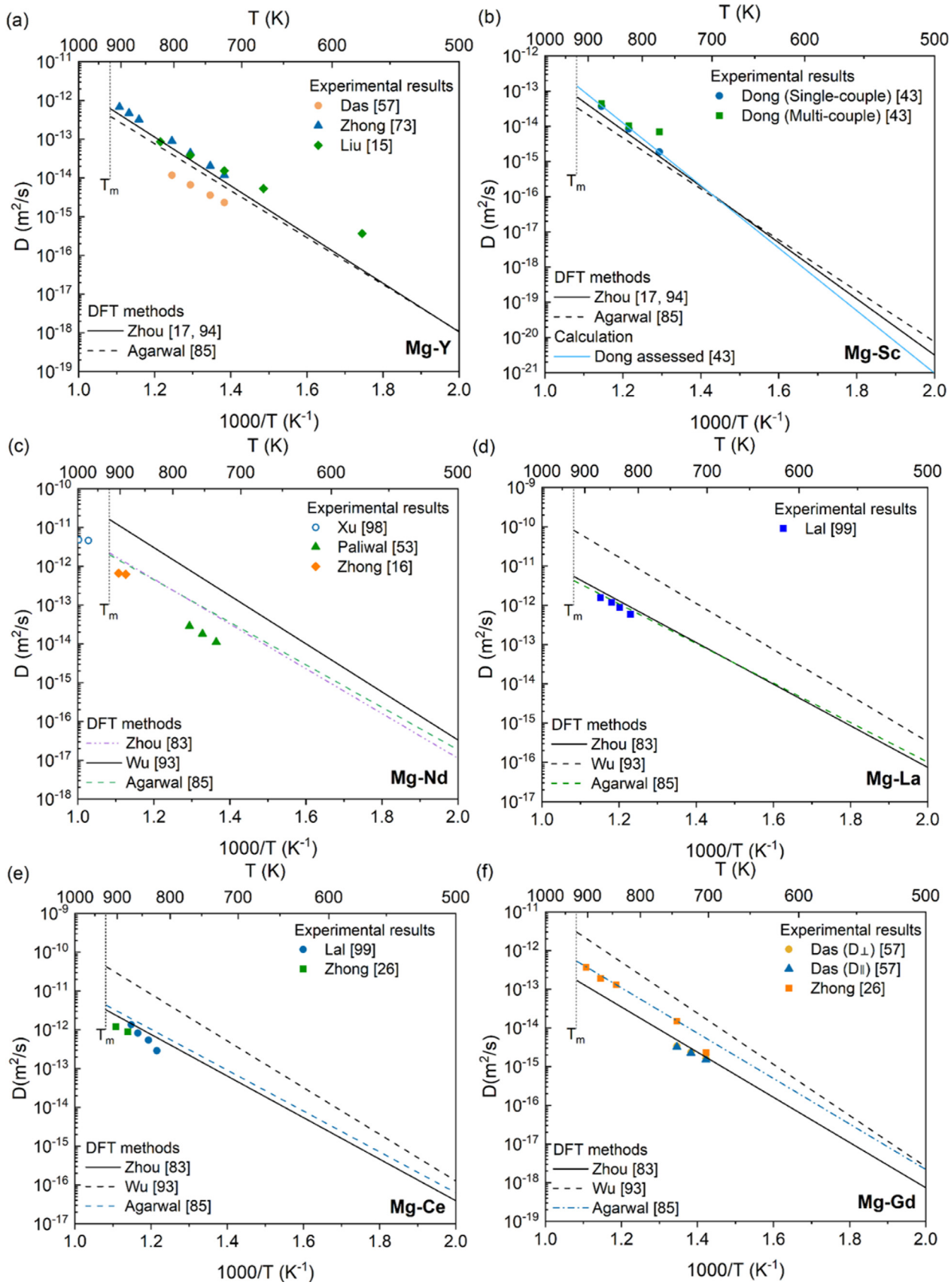

Fig. 2. Impurity diffusion coefficients of main addition RE elements [15–17,26,43,53,57,73,83,85,93,94,98,99] (a) Y, (b) Sc, (c) Nd, (d) La, (e) Ce and (f) Gd in hcp Mg.

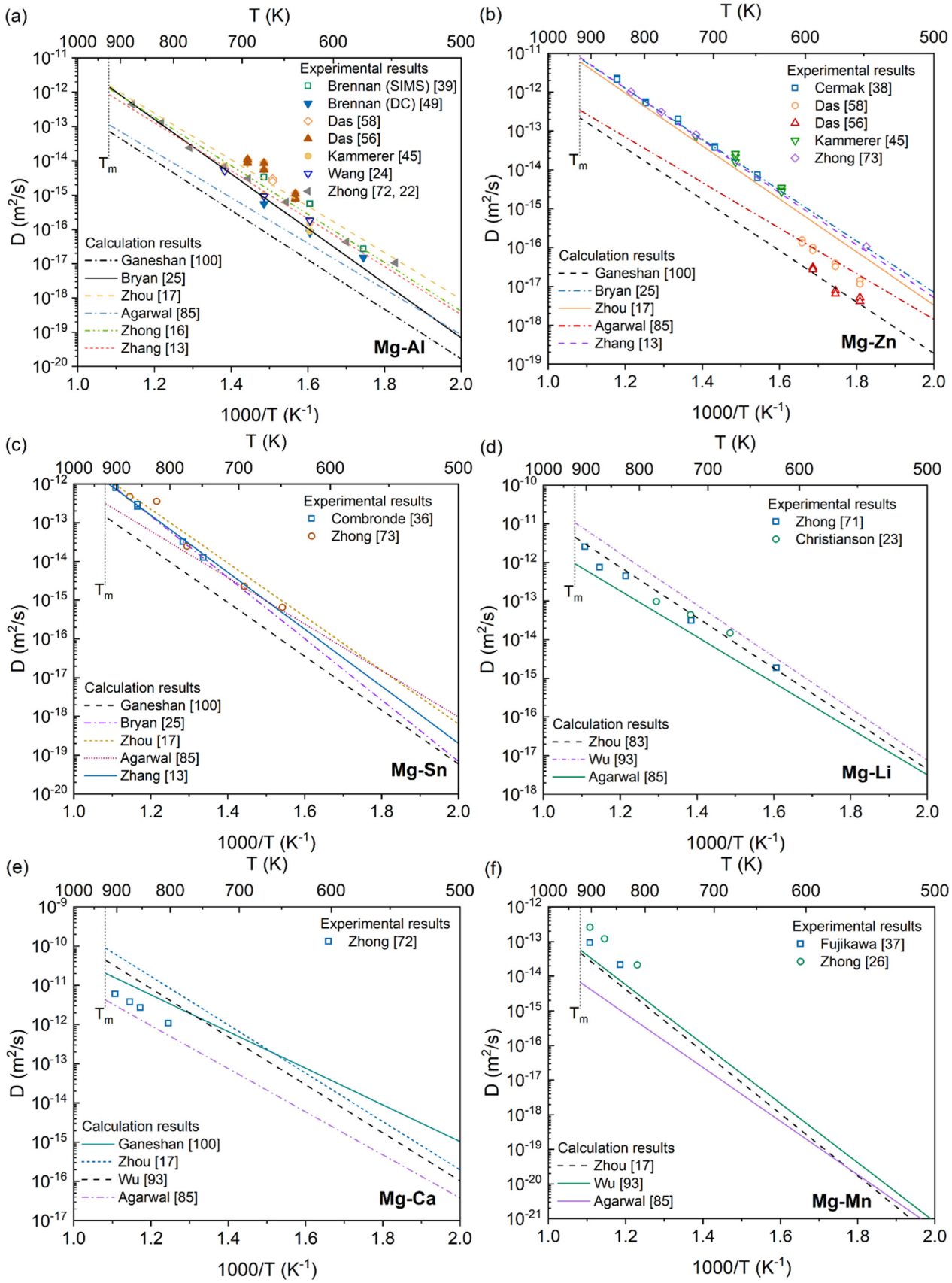

Fig. 3. Impurity diffusion coefficients of common elements [13,16,17,22–26,36–39,45,49,56,58,71–73,83,85,93,100] (a) Al, (b) Zn, (c) Sn, (d) Li, (e) Ca and (f) Mn in hcp Mg.

surface roughness occurred during the sputtering process was mentioned [39] as a significant factor which led to uncertain results. In addition, it can be easily found that diffusivities measured by Das et al. [56,58] in Fig. 3(a) were even larger. Therefore, they would not be included when assessing the impurity diffusion coefficients of Al in hcp Mg. Ganeshan et al. [100] made the first attempt to calculate the diffusion coefficients using DFT methods. The most important parameters correlation factors are relatively large for elements Al, Zn and Sn, which cause the calculated results to be one order of magnitude lower. So reliable impurity diffusivities of Al in Mg can be acquired by re-assessing diffusion data in literature except [39,56,58,100]. The way to obtain reasonable impurity diffusivities of Zn in Mg is similar to Al. The data from [25,38,45,73,94] can be used to evaluate the impurity diffusion data, excluding other controversial results.

The impurity diffusivities of Sn in Mg were also measured using both tracer method [36] and diffusion couple [73]. Fig. 3(c) indicates that these two sets are very close, which can directly be used to assess diffusion data without considering calculation results. It is noteworthy that Zhang et al. [13] performed assessment by DICTRA software package and obtained the diffusion data extremely close to experimental results. For Li (Fig. 3(d)), Zhong and Zhao [71] and Christianson et al. [23] determined its impurity diffusion coefficients by liquid-solid diffusion couple and solid-solid diffusion couple, respectively. The results from [83] matched well with diffusion data from Zhong and Zhao [71] and Christianson et al. [23]. Hence, their work [83] can be taken into account, but experimental data should be significantly emphasized. As pure Ca cannot be used for preparing diffusion couples, there is only one set of impurity diffusion data of Ca in Mg reported by Zhong and Zhao [72]. Moreover, there are also little experimental diffusion data for element Mn [26,37]. Despite the fact that there is no sufficient diffusion data, the reasonable impurity diffusivities of Ca and Mn in Mg still need to be improved depending more on experiments. Similarly, assessing impurity diffusion data for elements Be, Fe, Ni, Cu, Ga, Ag, Cd, In, Sb, U and Pu [36,50,99,101–104] in Fig. 4 should focus more on experiments. For the other elements without experimental data (marked in light blue), the diffusion coefficients can be gained by analyzing DFT data. In a brief summary, diffusion of 67 elements has been investigated by researchers using tracer method, SIMS method, diffusion couple or/and first principle calculations. The effective way to obtain the reasonable diffusivities of these elements in Mg can be concluded as: considering the reliability of experimental and calculated methods when screening the available data, and then concentrating more on experimental data. All the elements with experimental diffusion data are summarized in this work, which is presented in Fig. 5.

3.2.3. Influence of temperature and additional alloying elements on impurity diffusion data in Mg

The impurity diffusion coefficients of the aforementioned rare earth elements (Fig. 2) and some common elements (Fig. 3) in hcp Mg at elevated temperatures have a higher value than that at low temperatures. The temperature dependence of the impurity diffusion coefficients for these elements in hcp Mg can all be described using Arrhenius relation. However, impurity diffusivities measured over a narrow temperature interval cannot determine the pre-exponential factor and activation energy precisely. For that reason, assessment of impurity diffusion coefficients should rely on more experimental data over a relatively wide temperature range. Interestingly, it is easy to be found in Figs. 2–5 that impurity diffusion data in hcp Mg has not been obtained experimentally at lower temperatures (especially below 523 K) owing to sluggish diffusion. This phenomenon also confirmed that impurity diffusion coefficients of alloying elements highly depend on temperature.

The impurity diffusion coefficients of Al, Zn, Sn and Ga in hcp Mg are described in details in the Section 3.2.2, which are independent on their own contents. To explore the influence of the content of additional alloying elements on impurity diffusivities, the impurity diffusion data in Mg–Al–Zn, Mg–Al–Sn and Mg–Al–Ga ternary alloys were compared with that in hcp Mg in this paper. Mg–Al–Zn is the most representative Mg ternary system, which was first studied by Čermák et al. [38]. The impurity diffusivities of Zn in Mg–Al primary solid solution were examined by tracer method over the range of 648–848 K. The impurity diffusivities of Zn in Mg–0 at.% Al [38] are close to that measured by Zhong and Zhao [73] and Kammerer et al. [45], as indicated in Fig. 3(b). Table 1 shows the impurity diffusion coefficients of Zn in Mg–Al alloys with different Al concentrations at different temperatures, suggesting that the value of impurity diffusivities of Zn increases slightly with the increase of Al concentration. Wang et al. [24] re-calculated the experimental data in [105] using the Hall method (listed in parentheses of the Table 1), and the impurity diffusivities of Al or Zn in hcp Mg were in accordance with experimental data in Fig. 3(a) and (b). As listed in Table 1, the re-calculated impurity diffusion coefficients of Al in Mg–Zn [24] deviate from that of Kammerer et al. [105] significantly, especially when the composition of Zn is low. The re-calculated impurity diffusion coefficients of Zn in Mg–Al [24], however, agree well with that in [105]. Although the impurity diffusion coefficients in Mg–Al–Zn ternary system are inadequate, it is evident that increasing Al and Mg promote their impurity diffusion coefficients in Mg–Zn and Mg–Al.

There was only one set of impurity diffusion coefficients in hcp Mg–Al–Sn and Mg–Al–Ga system. For Mg–Al–Sn system, the impurity diffusivities of Sn in hcp Mg–Al $D^{Mg}_{Sn(Mg-Al)}$ and Al in Mg–Sn system $D^{Mg}_{Al(Mg-Sn)}$ were analyzed by Zhou et al. [68] at 673 and 723 K. Fig. 6(a) shows the variation of these two values, illustrating that $D^{Mg}_{Sn(Mg-Al)}$ and $D^{Mg}_{Al(Mg-Sn)}$ have a strong connection with temperature. Nonetheless, it seems that they have little compositional dependence due to the effect of Al–Al and Sn–Sn pair by roughly considering impurity diffusion data in Fig. 6(a). Zhou et al. [20] also investigated the evolution of $D^{Mg}_{Al(Mg-Ga)}$ and $D^{Mg}_{Ga(Mg-Al)}$ values with the increase of Ga content and Al content at 673 and 723 K, respectively. The

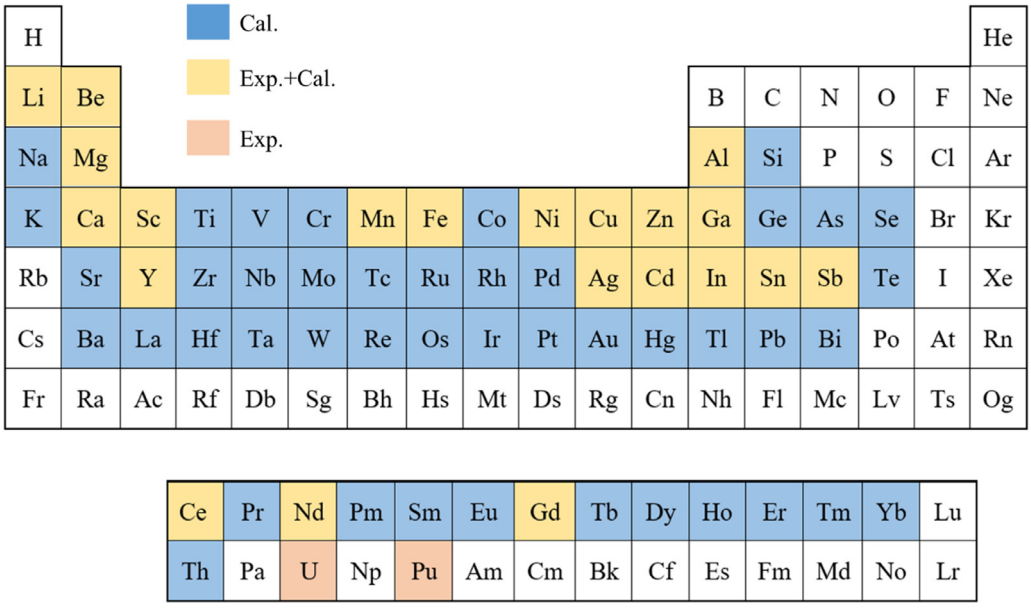

Fig. 4. Diffusion of 67 alloying elements was investigated in literature for impurity diffusivities donated in the periodic table.

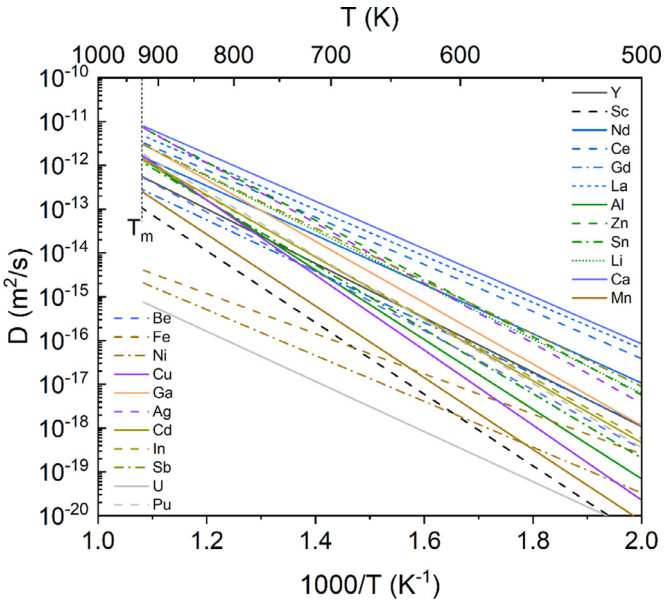

Fig. 5. Summary of the evaluated values of impurity diffusion coefficients for alloying elements investigated experimentally in Mg.

impurity diffusion coefficients of Al and Ga in Mg at these two temperatures were also depicted in Fig. 6(b), demonstrating that $D^{Mg}_{Al(Mg-Ga)}$ and $D^{Mg}_{Ga(Mg-Al)}$ increase with increasing Ga and Al concentration.

3.3. Inter-diffusion coefficients in binary and ternary Mg alloys

Diffusion couples are the main methods for determining inter-diffusion coefficients in Mg binary and ternary systems, which are indispensable for better understanding the diffusion controlled processes in terms of alloys preparation, heat treatment and service periods. However, the inter-diffusivity data in Mg alloys are scarce, compared with their impurity diffusion coefficients. For binary systems, only inter-diffusivities of elements Al, Zn, Sn, Li, Mn, Ce, Y, Gd, Nd, Sc, Dy, Cu and Pr were investigated. Inter-diffusion coefficients $\tilde{D}_{Mg--Al}$ and $\tilde{D}_{Mg--Zn}$ were studied by several researchers, whose experimental data are shown in Fig. 7. Note that the inter-diffusion coefficients basically shows an upward trend with the increase of Al and Zn content at all temperatures, which can explain that the melting points of hcp Mg solid solution decrease with the addition of Al and Zn. Mg alloys with higher inter-diffusion coefficients will possess the lower activation energy, and thus weak bonding strength among atoms. The melting points of alloys then decrease since they are in proportion with bonding strength. Obviously, the inter-diffusion coefficients in hcp Mg with Zn are approximately an order of magnitude higher than those in hcp Mg with Al at the same temperature. $\tilde{D}_{Mg--Al}$ increases much more quickly with Al addition, compared to the increase rate of $\tilde{D}_{Mg--Zn}$ with Zn addition. The inter-diffusion coefficients for the other alloying elements are not summarized in this paper, since there exists only one set of data for each system. In more details, when assessing the binary interaction parameters $\Phi^{Mg,X}_{X}$, experimental inter-diffusion coefficients should be determined at more than three temperatures and over a relatively wide composition range [16].

In Mg ternary alloys, the main (direct) inter-diffusion coefficients ($\tilde{D}^{k}_{ii}$ and $\tilde{D}^{k}_{jj}$) and cross (indirect) inter-diffusion coefficients ($\tilde{D}^{k}_{ij}$ and $\tilde{D}^{k}_{ji}$) are extracted from the compositional profiles, which denote the effect of concentration gradient of one alloying element on the diffusion rate of the same element and other elements in the presence of a third element,

Table 1
Impurity diffusion coefficients of Al in Mg–x at.% Zn solid solution $D^{Mg}_{Al(Mg--Zn)}$ at 673 and 723 K, and Zn in Mg–x at.% Al solid solution $D^{Mg}_{Zn(Mg--Al)}$ over the range of 648–848 K [24,38,105].

T (K)	$D^{Mg}_{Al(Mg--Zn)}$	Value (m^2/s)	T (K)	$D^{Mg}_{Zn(Mg--Al)}$	Value (m^2/s)
648			648	$D^{Mg}_{Zn(Mg--1.60Al)}$	1.00×10^{-14} 1.16×10^{-14}
				$D^{Mg}_{Zn(Mg--3.53Al)}$	1.19×10^{-14} 1.41×10^{-14}
				$D^{Mg}_{Zn(Mg--8.18Al)}$	1.43×10^{-14} 1.49×10^{-14}
673	$D^{Mg}_{Al(Mg--0.02Zn)}$	1.71×10^{-15}	673	$D^{Mg}_{Zn(Mg--2.70Al)}$	9.11×10^{-15} (6.75×10^{-15})
	$D^{Mg}_{Al(Mg--1.00Zn)}$	2.92×10^{-15} (5.28×10^{-16})		$D^{Mg}_{Zn(Mg--8.18Al)}$	4.81×10^{-14} 4.71×10^{-14}
	$D^{Mg}_{Al(Mg--2.10Zn)}$	2.06×10^{-15}		$D^{Mg}_{Zn(Mg--9.10Al)}$	3.35×10^{-14}
698			698	$D^{Mg}_{Zn(Mg--1.60Al)}$	5.70×10^{-14} 5.38×10^{-14}
				$D^{Mg}_{Zn(Mg--3.53Al)}$	6.37×10^{-14} 6.82×10^{-14}
				$D^{Mg}_{Zn(Mg--8.18Al)}$	9.27×10^{-14} 1.02×10^{-13}
723	$D^{Mg}_{Al(Mg--1.00Zn)}$	2.69×10^{-14} (1.61×10^{-14})	723	$D^{Mg}_{Zn(Mg--2.80Al)}$	5.80×10^{-14} (4.08×10^{-14})
	$D^{Mg}_{Al(Mg--2.00Zn)}$	5.56×10^{-14}		$D^{Mg}_{Zn(Mg--8.10Al)}$	1.49×10^{-13}
				$D^{Mg}_{Zn(Mg--8.18Al)}$	2.17×10^{-13} 2.36×10^{-13}
748			748	$D^{Mg}_{Zn(Mg--1.60Al)}$	2.35×10^{-13} 2.61×10^{-13}
				$D^{Mg}_{Zn(Mg--3.53Al)}$	2.61×10^{-13} 2.82×10^{-13}
				$D^{Mg}_{Zn(Mg--8.18Al)}$	1.08×10^{-12} 1.44×10^{-12}
798			798	$D^{Mg}_{Zn(Mg--1.60Al)}$	6.91×10^{-13} 6.84×10^{-13}
				$\tilde{D}^{Mg}_{Zn(Mg--3.53Al)}$	6.75×10^{-13} 6.81×10^{-13}
848			848	$D^{Mg}_{Zn(Mg--1.60Al)}$	2.36×10^{-12} 2.30×10^{-12}
				$D^{Mg}_{Zn(Mg--3.53Al)}$	2.64×10^{-11} 2.55×10^{-11}

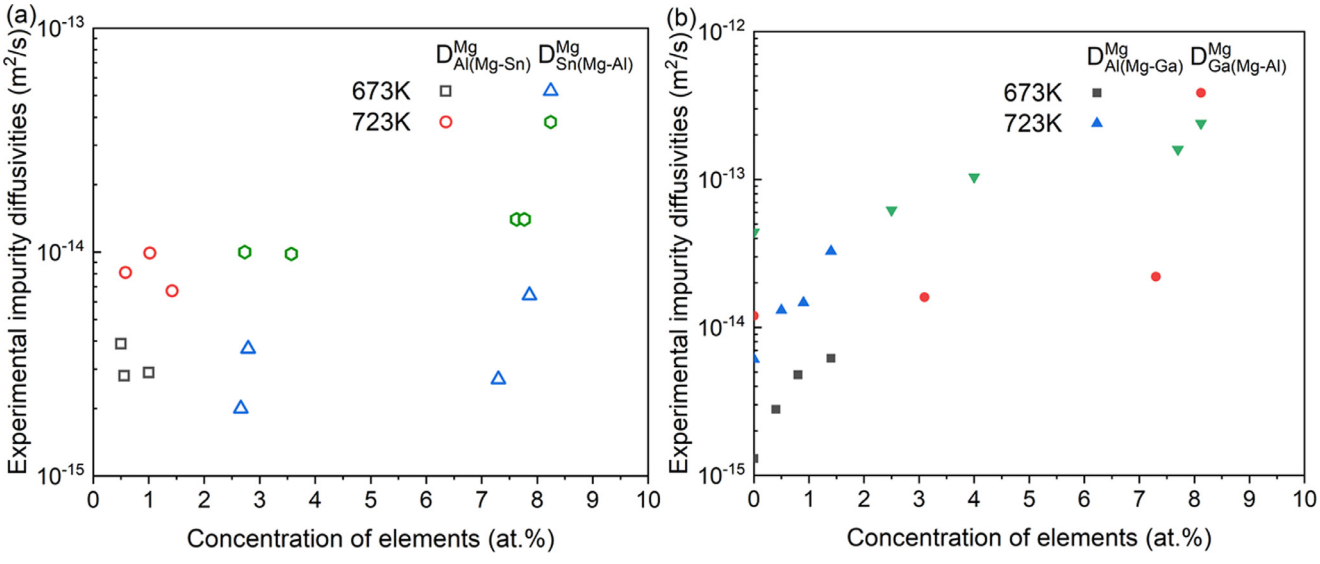

Fig. 6. Impurity diffusion coefficients of (a) Al in hcp Mg–Sn and Sn in hcp Mg–Al system [68] and (b) Al in hcp Mg–Ga and Ga in hcp Mg–Al [20].

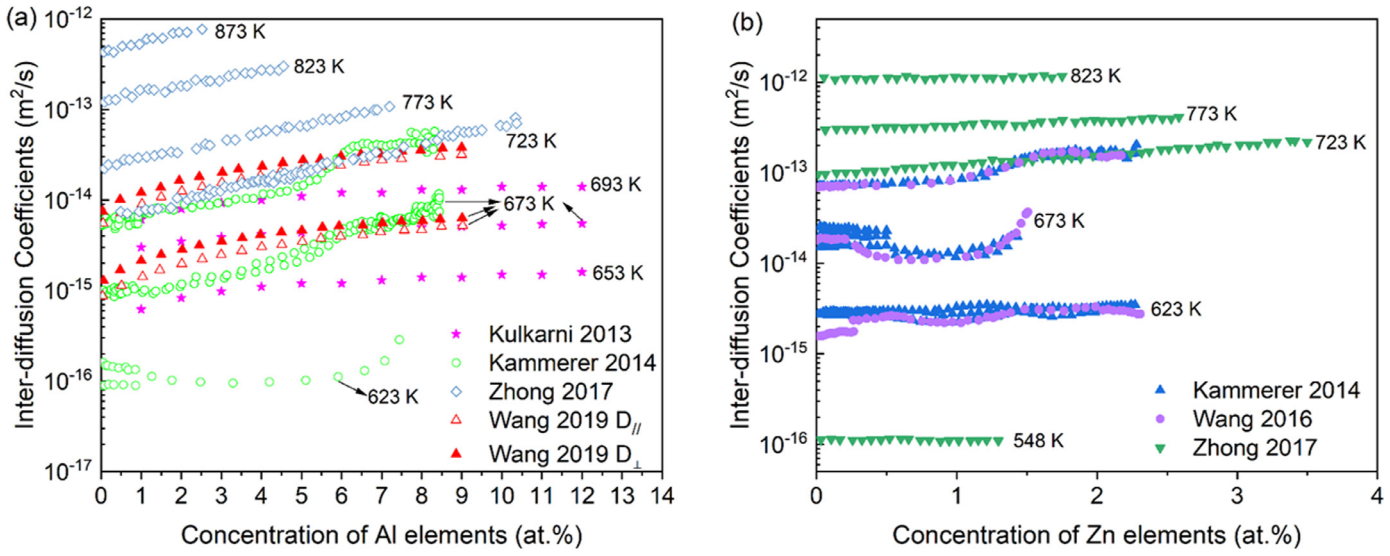

Fig. 7. Inter-diffusion diffusion coefficients of (a) Mg–Al at the low Al concentration range [45,46,60,72] and (b) Mg–Zn at the low Zn concentration range [24,45,73].

respectively [21,106]. These two types of inter-diffusion coefficients in Mg–Al–Zn, Mg–Al–Sn, Mg–Al–Ga and Mg–Al–Li were reported in [20,21,23,68,107]. Their corresponding atomic mobility parameters were assessed on the basis of diffusion data in sub-binary systems, ternary inter-diffusion coefficients together with thermodynamic descriptions.

Apart from aforementioned diffusion coefficients in Mg alloys, information on grain boundary diffusion is also important. However, only the activation energy for grain boundary diffusion (92 kJ/mol) in pure Mg was proposed by Frost [108]. Besides, GB diffusion coefficients of Al [55], Zn [38], Ga [109] and Ge [110] in Mg has been measured so far. Nonetheless, there is merely a single set of GB diffusion coefficients for each element. The specific GB diffusion coefficients are not concluded in this work, owing to inadequate information from literatures.

4. Practical applications of diffusion coefficients in Mg alloys

4.1. Assessment of atomic mobility for Mg based alloys

In general, diffusion coefficients depend significantly on compositions and temperatures, which makes these data complex and massive, especially in multi-component Mg systems. Atomic mobility, establishing based on diffusion coefficients, are modelled for providing the diffusion information of Mg alloys. According to the theory of Andersson and Ågren [111], the atomic mobility M_B for element B could be divided into two main parts, the frequency factor M_B^0 and activation energy Q_B, which would be expressed as following:

$$M_B = M_B^0 \exp\left(\frac{-Q_B}{RT}\right)\frac{1}{RT} = \exp\left(\frac{RTlnM_B^0}{RT}\right) \exp\left(\frac{-Q_B}{RT}\right)\frac{1}{RT} \quad (3)$$

where R is the gas constant. Both $RTlnM_B^0$ and Q_B are dependent on composition, temperature and pressure, and they can be grouped into one parameter $\phi_B = -Q_B + RTlnM_B^0$. This single parameter can be expanded on the basis of the CALPHAD in the Redlich-Kister polynomials as:

$$\phi_B = \sum_p x_p \phi_B^p + \sum_p \sum_{q>p} x_p x_q \left[\sum_{r=0,1,2,\ldots} {}^r\phi_B^{pq}\left(x_p - x_q\right)^r\right] + \sum_p \sum_{q>p} \sum_{v>q} x_p x_q x_v \left[\sum_{s=p,q,v} {}^s\phi_B^{pqv}\left(x_s + \frac{1 - x_p - x_q - x_v}{3}\right)\right] \quad (4)$$

where ϕ_B^P is the value of ϕ_B, x_p and x_q denote the mole fraction of element p and q, binary and ternary interaction parameters are given by ϕ_B^{pq} and ϕ_B^{pqv}, respectively.

To the best of our knowledge, current reliable atomic mobility of Mg systems follows the traditional procedure, which starts from the comprehensive review of various diffusion coefficients. Meanwhile, the assessment of atomic mobility database for Mg alloys is merely concentrated on binary and several ternary systems resulting from limited ternary or high-order diffusion data in hcp Mg. Zhong and Zhao [16] has concluded and assessed 22 binary Mg–X systems. Take Mg–Zn binary system as an example [13,16,24], ϕ_{Mg}^{Mg}, ϕ_{Zn}^{Mg}, ϕ_{Zn}^{Zn} were firstly fixed according to self-diffusivity of hcp Mg, impurity diffusivity of Zn in hcp Mg, self-diffusion coefficients of Zn, as exhibited in Section 3. For lack of sufficient data, the impurity diffusivity of Mg in Zn (for obtaining ϕ_{Mg}^{Zn}) was assumed to equal to self-diffusivity of Zn when the content of Zn approached to 1. Then $\phi_{Zn}^{Zn,Mg}$ was retrieved from inter-

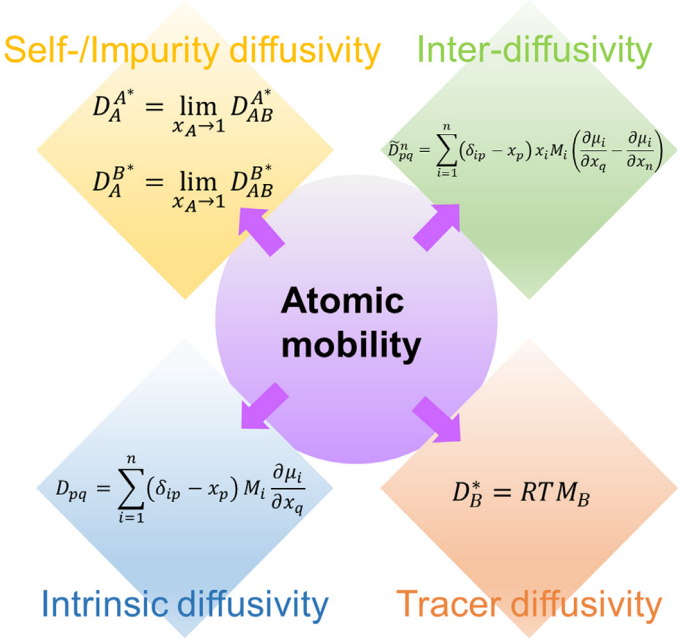

Fig. 8. Relationship between atomic mobility database and different types of diffusion coefficients.

diffusion coefficients in the hcp phase. Zhang et al. [13] also re-assessed the atomic mobility of Mg–Al and Mg–Sn alloys over a wide composition range, which helped evaluate the atomic mobility for Mg–Al–Sn system [21]. $\phi_{Al}^{Sn,Mg}$ and $\phi_{Sn}^{Al,Mg}$ in Zhang et al. [21] are adjustable parameters according to the impurity diffusion coefficients of Al in hcp Mg–Sn and Sn in hcp Mg–Al obtained from two different ternary diffusion studies. Even though many attempts have been made by fellows, the diffusional mobility of only four hcp ternary systems, Mg–Al–Sn [16,21,112], Mg–Al–Zn [16,21,24], Mg–Al–Ga [20] and Mg–Al–Li [23] were assessed. Narrow experimental ternary diffusion data and uncertainties in evaluating the interaction parameters add the difficulties in establishing the atomic mobility of high-order Mg systems. A novel computational framework for assessing diffusional mobility directly from its composition profiles was proposed by Zhong et al. [113]. It definitely provided an assistant idea for obtaining mobility database, however, it has not been applied in Mg systems.

Once the atomic mobility and thermodynamic database are established, different types of diffusion coefficients over a wide range of temperature and composition can thus be derived [20]. As demonstrated in Fig. 8, various diffusion coefficients, i.e., tracer diffusion coefficients, inter-diffusion coefficients, etc., can be deduced from the related equations. It is worth pointing out that n is set as component dependent, δ_{ip} is the Kronecker delta (if i=p, δ_{ip}= 1, otherwise δ_{ip}= 0), μ_i and x_i is the chemical potential and the fraction of element i, respectively. The thermodynamic factor $\frac{\partial \mu_i}{\partial x_i}$ can be easily obtained from thermodynamic database. In addition, mobility database can be utilized for precisely predicting the diffusion-controlled process, which will be discussed in Sections 4.2 and 4.3.

4.2. Simulation of precipitation evolution for Mg based alloys

Precipitation simulation of Mg alloys can reasonably optimize their mechanical properties by virtue of predicting characteristic of precipitates, including size, number density, volume fraction and particle size distribution. Many simulation tools, for example, MatCalc [114], PanPrecipitation [112,115–117], PrecipiCalc [118,119], and TC-PRISMA [13,120] have been developed to simulating the precipitation evolution, combined with reliable thermodynamic database and assessed atomic mobility. Among these tools, PanPrecipitation and TC-PRISMA were adopted in Mg systems. Kampmann-Wagner numerical (KWN) model [121] was chosen as the precipitation model, which is developed based on Langer-Schwartz theory [122].

Precipitation processes are composed of three stages, phase nucleation, growth and coarsening [123]. According to the classic nucleation theory (CNT), the nucleation rate $J(t)$ is calculated by:

$$J = N_V Z \beta^* \exp\left(-\frac{\Delta G^*}{kT}\right) \exp\left(\frac{-\tau}{t}\right) \tag{5}$$

where Z is the Zeldovich factor, β^* is the atomic attachment rate, N_v is the density of nucleation site, k is the Boltzmann constant, T is the temperature, t is the time, τ is the incubation time, ΔG^* is the activation free energy required for the formation of a stable nucleus. The nucleation rate has a strong relationship with system thermodynamics, since the key component, driving force energy for generating precipitate from the matrix could be calculated from a reliable thermodynamic database.

The growth rate for spherical particles under the diffusion-controlled assumptions, where Gibbs-Thompson effect is also considered, is simply given as:

$$v = \frac{dr}{dt} = \frac{2\sigma V_m^{\beta} K}{R}\left(\frac{1}{R^*} - \frac{1}{R}\right) \tag{6}$$

where R and R^* are the radii of the practical and critical nuclei, respectively. σ is the interfacial energy between α-Mg and β-precipitate, and V_m^{β} is the molar volume of the precipitate phase β. K is kinetic parameter, which can be described with solute composition and mobility as:

$$K = \left[\sum_i \frac{\left(x_i^{\beta/\alpha} - x_i^{\alpha/\beta}\right)^2 \xi_i}{x_i^{\alpha/\beta} M_i}\right]^{-1} \tag{7}$$

where $x_i^{\beta/\alpha}$ and $x_i^{\alpha/\beta}$ are the solute composition of precipitate and matrix at the interface of precipitate and matrix, respectively. M_i is the atomic mobility of the solute element i in the α-Mg phase. ξ_i is a factor for adjusting the effective diffusion distance as the supersaturation varies [124]. For non-spherical particles [120], additional pre-factors will be added to optimize Eq. (6).

In line with the aforementioned theory, kinetic parameters are also required for performing precipitation simulation

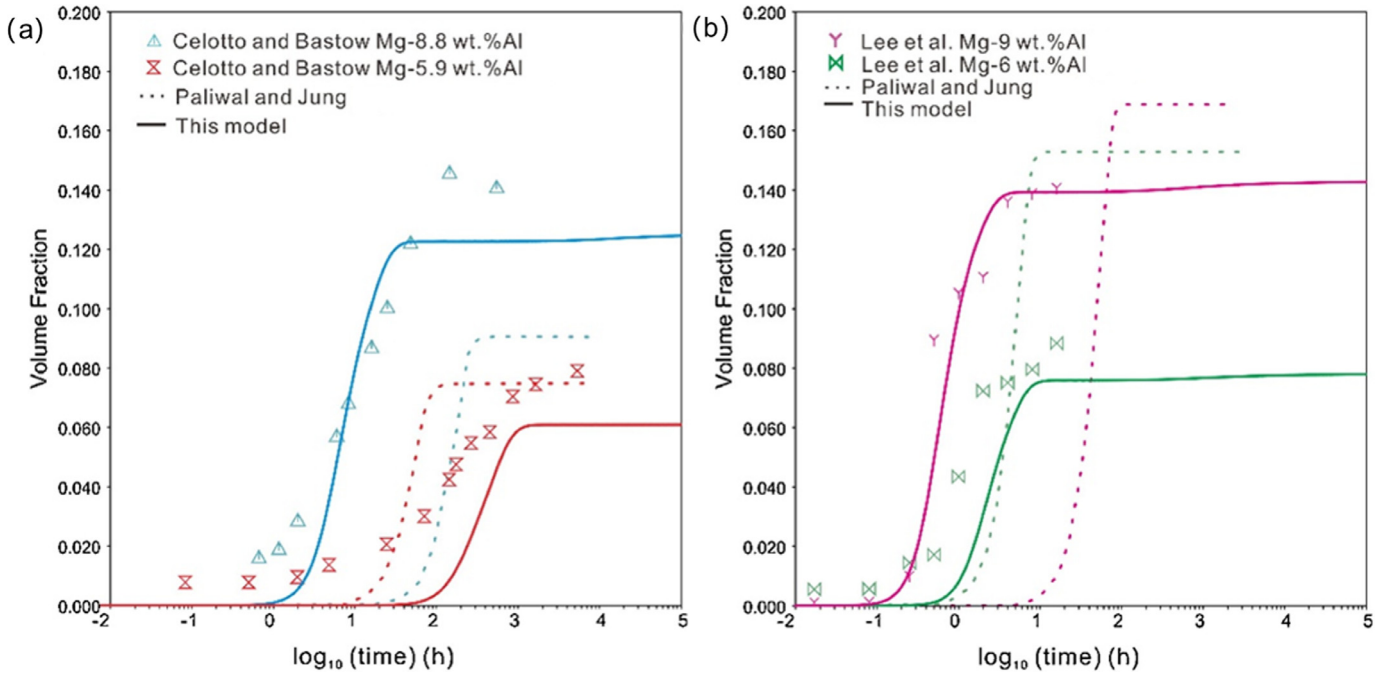

Fig. 9. Volume fraction of precipitate γ-$Mg_{17}Al_{12}$ (a) in Mg–8.8 wt.% Al and Mg–5.9 wt.% Al alloys at 473 K and (b) in Mg–9 wt.% Al and Mg–6 wt.% Al alloys at 443 K from experiments and simulation [13].

except from thermodynamic database and diffusional mobility. The parameters, nucleation site, molar volume of α-Mg and precipitate, and interfacial energy, would be used in the simulation. Zhang et al. [116] predicted the microstructural evolution of γ-$Mg_{17}Al_{12}$ phase in AZ91 alloy, which is accordance with the experimental results in Celotto [125]. Sun et al. [112] also predicted the number density and radius of Mg_2Sn phase in Mg–1.3 at.% Sn and Mg–1.9 at.% Sn at 473 K, showing good agreement with measured values in Mendis [126]. Additionally, Xia et al. [117] utilized the built-in atomic mobility database in PanPrecipitation module accurately obtained β-precipitate in Mg–Sm–Zn–Zr alloy with responsible modified kinetic parameters, an idea that was also used in their subsequent work [14] with assessed atomic mobility parameters of Mg–Zn–Nd alloy.

Zhang et al. [13] assessed the atomic mobility of Mg–Al, Mg–Zn and Mg–Sn systems and then performed simulation of precipitation behavior based on assessed mobility data and reliable thermodynamic data using TC-PRISMA tool. The volume fraction of precipitate γ-$Mg_{17}Al_{12}$ in Mg–8.8 wt.% Al and Mg–5.9 wt.% Al alloys at 473 K (Fig. 9(a)) and in Mg–9 wt.% Al and Mg–6 wt.% Al alloys at 443 K (Fig. 9(b)) were simulated in their work, which were nearly in agreement with experimental data from Celotto and Bastow [127] and Lee et al. [128], respectively. It is noticeable that the simulated results from Paliwal and Jung [27] were far from experimental data, and it may result from poor reproduction of the nucleation stage. Thereby, reasonable precipitation simulation work based on assessed atomic mobility provides reliable specific information of precipitate.

4.3. Prediction for mechanical properties of Mg based alloys

For further practical application, atomic mobility database would also be useful for predicting the mechanical properties of Mg alloys. The precipitation evolution of Mg alloys obtained from atomic database can be predicted using the method described in Section 4.2, which would help calculate the strength increment during the precipitation process and thus optimize their heat treatment process.

The overall yield strength can determined according to the rule of additions and expressed as [115]:

$$\sigma_y = \sigma_0 + \sigma_{gb} + \sigma_{ss} + \sigma_p \tag{8}$$

where σ_0 is the intrinsic strength of α-Mg. σ_{gb} is the strength resulting from grain boundary hardening, and would not change during ageing process. Sun et al. [129] and Liu et al. [130] confirmed that the grain size stayed stable at different ageing stages, indicating that the contribution of grain boundary strengthening would not alter. σ_{ss} originates from the solid solution strengthening, which depends on the mean solute concentration of each alloying element [115,131]. The forming of precipitates would consume the solute atom in the matrix, and hence the influence of the solid solution strengthening decreases with the ageing time prolonging. σ_p is the precipitation strengthening term, where shearing and bypassing are the main mechanisms for impeding dislocations. The contribution of precipitation strengthening can be estimated using the obtained precipitation information. Zhang et al. [116] reasonably estimated the overall yield strength of AZ91 alloy in virtue of its thermodynamic description, atomic mo-

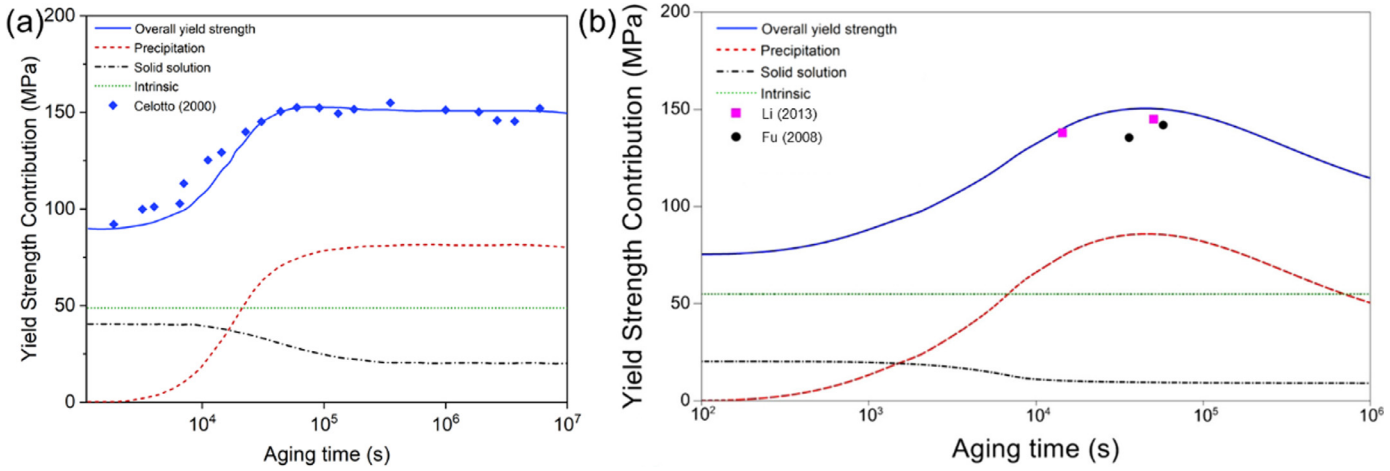

Fig. 10. Predicted strengthening contributions and yield strength of (a) AZ91 alloy compared to experimental data in [125] and (b) Mg–3Nd–0.2Zn alloy compared to data in [133,134] at 473 K.

bility and kinetic parameters. Experimental yield strength in Fig. 10(a) is calculated in this work from experimental Vickers hardness in [125], since Vickers hardness (HV) could be theoretically deduced from yield strength (MPa) [132] as:

$$HV = c(\sigma_y + \Delta) \tag{9}$$

where c is the elastic constraint factor, Δ represents the increase in flow stress arising from the strain hardening. The parameters c and Δ are constant for same material, which can be determined by fitting several experimental data. The similar positive outcome has been shown in Fig. 10(b) [14], indicating that diffusion coefficients serve as one of the most significant inputs for elucidating composition-microstructure-mechanical property relationships of Mg alloys.

Creep resistance is another representative mechanical property, which can be considered as an important criterion for determining the serviceability of Mg alloys in practical applications [135]. Diffusion is one of the most essential processes controlling the creep behavior of Mg alloys [136]. Even though the activation energies of diffusion have different physical meaning from that of creep behavior, the creep resistance of Mg alloys can be related with their diffusion data through activation energies value. Fig. 11(a) [137] presents the deformation mechanism of metal materials, revealing diffusion properties show strong link with creep behavior of Mg alloys at elevated temperatures over 0.5 T_m and very low stresses. The corresponding diffusional creep mechanism can be divided into several types, Nabarro-Herring (N-H) creep [138], Coble creep [139] and pipe diffusion [140], occurring through crystal lattice, only along grain boundary and preferentially along dislocation cores, respectively. Nonetheless, both compressive and tensile creep behavior of Mg alloys were operated at moderate temperatures [141] by most researchers, which cannot meet the requirements for diffusional creep. According to these theories and reproduced rate-controlled creep mechanism for Mg alloys in Fig. 11(b) [142], it seems that the diffusional creep mechanism is the secondary importance compared with other creep mechanisms [140].

For pure Mg, the activation energy value Q for creep is very similar to that for self-diffusion at very high temperatures [140], showing that creep strain results directly from the movement of Mg atoms [136]. Thus, self-diffusion coefficients of pure Mg shown in Section 3.1 can be applied in theoretical analyses. Zhang et al. [143] observed the creep behavior of as-extruded GW83 alloy under the stress of 40–70 MPa at 443–473 K (about 0.5 T_m) and reported that the primary tensile creep mechanism was Mg self-diffusion. Creep activation energy of dual-phases MA21 alloy was determined experimentally by Zhang et al. [144] as 123 kJ/mol at 373–423 K (about 0.45–0.5 T_m) under 30 MPa. The creep Q value of MA21 alloy would increase smoothly with the increase of temperatures, which was very close to the activation energies for Mg self-diffusion and/or Al self-diffusion. Hence, the creep rate of MA21 alloy at relatively elevated temperatures would depend on the dislocation blocking behavior caused by diffusion of Mg and/or Al atoms. In addition, Ouyang et al. [145] extracted the creep Q value of T4 and T6 state Mg–15 wt.% Gd alloy below and above 533 K (about 0.5 T_m) under 50 MPa and the value of Q is 141 kJ/mol at high temperatures. It is consequently suggested that the creep mechanism of Mg–15 wt.% Gd alloy would be dependent on the diffusion of Gd in Mg. The conclusion in [145] may be inferred from the theory in [72] that fast diffusion rate of solute atoms in hcp Mg will lead to poor creep resistance of Mg-based alloys. However, sufficient explanations has not been given in Ouyang et al. [145]. Furthermore, high impurity diffusion coefficients of Ca in Mg (Fig. 3(e)) cannot explain the fact that creep resistance of Mg–Ca alloys improved with the increase of Ca [142]. Wang et al. [146] confirmed futher that impurity diffusion of solute in Mg cannot determine the creep behavior of Mg alloys. Therefore, diffusion of Mg and/or alloying atoms has been taken as the mechanisms of their creep behavior through hindering dislocation moving.

Apart from relatively high temperatures, diffusional creep can also occur at low temperatures (about 0.4 T_m) and high stresses. The activation energy of pipe diffusion is consid-

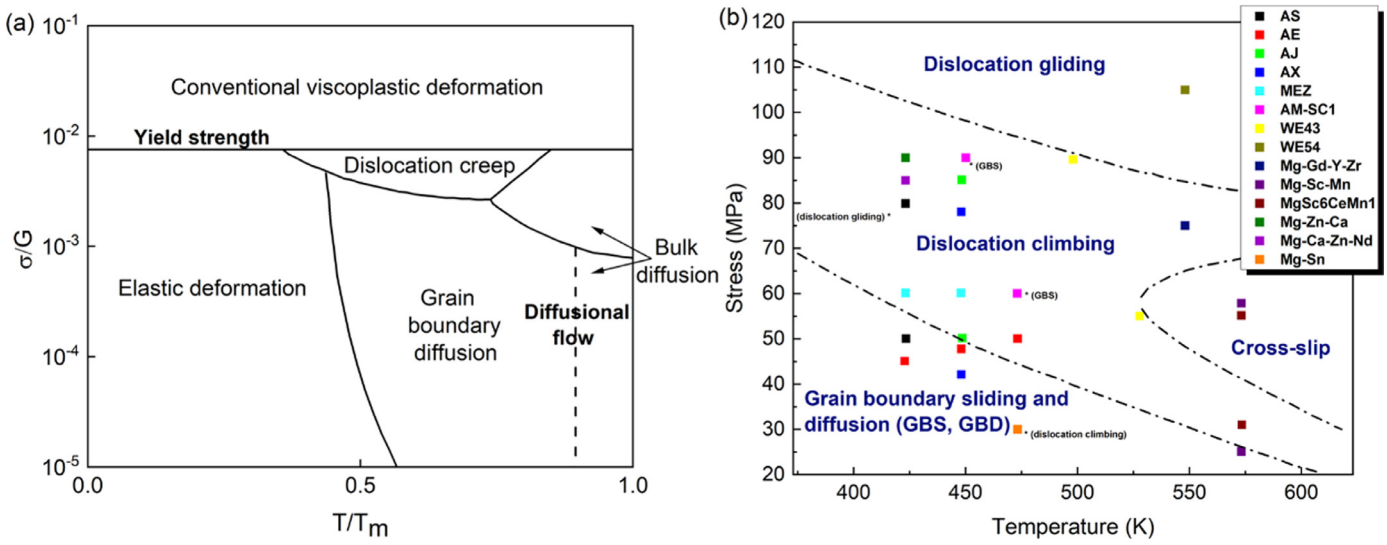

Fig. 11. (a) Deformation mechanism map [137] and (b) the distribution of the rate-controlling creep mechanisms for Mg alloys in a stress range of 20–120 MPa and temperature range of 373–623 K [142].

ered to be slightly higher than that of grain boundary diffusion of Mg. There is only one set of activation energy for grain boundary diffusion in pure Mg (92 kJ/mol) [108], differing from diffusion data summarized in Section 3 but providing a reference to analyzing the creep mechanisms of Mg alloys. The creep activation energy for AZ91 alloys and Sn-containing AZ91 alloys were detected by Mahmudi and Moeendarbari [147] as 110 kJ/mol at 600 and 650 MPa in the 423–523 K range, which could be connected with pipe diffusion. The dominate creep mechanism of as-cast MRI153 magnesium alloys was also inferred as pipe diffusion, considering that the average Q value were in the range of 99.5–115.2 kJ/mol at the temperatures between 425 and 490 K with applied stress from 360 to 600 MPa [148]. The same pipe diffusion controlled creep rate mechanism was also confirmed in Sn-containing MRI153 Mg alloys by Nami et al. [149]. The creep mechanisms of AZ61 alloys [150], Ca and Sb added AZ91 alloys [151] and AZ81 alloys [152] at high stresses and low temperatures were all suggested to be pipe diffusion in that the average creep activation energies were marginally higher than activation energy for pipe diffusion. That is to say, the creep mechanism could be revealed through comparing the creep activation energies and diffusion activation energies extracted from diffusion data. Another activation energy for lattice diffusion of Mg (135 kJ/mol) [108, 153] is used for determining the creep mechanism at relatively low stresses and temperatures. For instance, average creep activation energies of Sn added AZ91 alloys were obtained in Mahmudi and Moeendarbari [147] as 125–150 kJ/mol under 150 MPa, implying that the creep rate were controlled by lattice diffusion at relatively stresses. Some Mg alloys achieved the transition from lattice diffusion to pipe diffusion controlled creep mechanism by increasing applies stresses [152,154]. All these studies indicate that determining the relationship between diffusion data and creep resistance of Mg alloys help design Mg based alloys with high creep performance. The diffusion data which are deemed to be useful in analyzing creep mechanisms of Mg alloys are listed in the Section 3.

5. Conclusions and remarks

5.1. Summary

In summary, experimental measuring and feasible calculated methods are well-developed for determining diffusion coefficients precisely. Diffusion data of rare earth elements and some common elements in Mg systems are reviewed in this article for establishing atomic mobility database within the CALPHAD spirt. Different types of diffusion coefficients over a wide temperature and composition range can be deduced from reliable atomic mobilities of Mg alloys. Panprecipitation and TC-PRISMA are two main simulation tools for predicting precipitation behavior of Mg alloys through combining thermodynamic database, diffusional mobility database with kinetic parameters. The number density, size, volume fraction and particle size distribution of precipitates in Mg alloys can be well predicted using the precipitation simulation. Furthermore, overall yield strength and corresponding hardness for ageing Mg alloys will be calculated accurately since the precipitation strengthening dominates during the ageing process. The correlation of diffusion data and creep mechanisms of Mg alloys are also reviewed in detail, which provides insight into their creep behavior. Thus, the diffusion coefficients could serve as one key input for connecting composition-microstructure-mechanical properties.

5.2. Outlook and remarks

The review article herein provides an overview on exsting diffusion coefficients for Mg alloys and their correspond-

ing applications. A seemingly complete connection has been established, while there is still a gap in this field. In the future, the key issue to expand further atomic mobility database for ternary or high order Mg alloys will be to improve the efficiency for determining diffusion coefficients. Preparation method, friction welding technology along with heat treatment process, could be an attempt to obtain better diffusion for Mg systems. Based on Fick's second law, the diffusional mobility could be assessed directly from high-throughput approach, where different types of diffusion coefficients would be calculated. Taking advantage of available diffusion data, high-throughput approach would be optimized continuously to reduce the uncertainty. In the end, the better agreement can be achieved between calculated composition profiles and experimental composition profiles.

Poor strength and creep resistance are still the backwards for Mg alloys. Precipitation simulation founded on diffusivities data is definitely significant for optimizing heat treatment process and thereby expecting optimum properties of Mg alloys. However, lack of atomic-scale investigations on mechanical properties of Mg alloys made it difficult to establish the connection mechanical performance with the diffusion of atoms, even with diffusion data. Thus, various *in-situ* observation technologies should be exploited to analyze the microstructural evolution, which would reveal the intrinsic mechanisms. Especially for creep behavior of Mg alloys at high temperatures and low stresses, researchers always point out the relationship between diffusion behavior and creep mechanisms theoretically, rather than experimental confirmation. It would also be the reason for misunderstanding the link between diffusivities and creep mechanisms. Further atomic-scale experimental exploration is essential, which will provide more specific and convincing evidence for understanding the mechanisms and predicting the mechanical performance.

Acknowledgments

This work was financially supported by the China Scholarship Council (Grant No: 202006890008), China, Science and Technology Committee of Shanghai (19010500400), the "111" project (D16002) and the Independent Research Project of State Key Laboratory of Mechanical Transmissions (Grant No. SKLMT-ZZKT-2021M11).

References

[1] Q. Luo, Y. Guo, B. Liu, Y. Feng, J. Zhang, Q. Li, K. Chou, J. Mater. Sci. Technol. 44 (2020) 171–190.
[2] T. Xie, H. Shi, H. Wang, Q. Luo, Q. Li, K.C. Chou, J. Mater. Sci. Technol. 97 (2022) 147–155.
[3] S. You, Y. Huang, K.U. Kainer, N. Hort, J. Magnes. Alloy. 5 (3) (2017) 239–253.
[4] Y. Xu, F. Gensch, Z. Ren, K.U. Kainer, N. Hort, Prog. Nat. Sci. Mater. Int. 28 (6) (2018) 724–730.
[5] Y. Ali, D. Qiu, B. Jiang, F. Pan, M.X. Zhang, J. Alloy. Compd. 619 (2015) 639–651.
[6] D. Wang, P. Fu, L. Peng, Y. Wang, W. Ding, Mater. Charact. 153 (2019) 157–168.
[7] J.H. Li, J. Barrirero, G. Sha, H. Aboulfadl, F. Mücklich, P. Schumacher, Acta Mater. 108 (2016) 207–218.
[8] D. Liu, D. Yang, X. Li, S. Hu, J. Mater. Res. Technol. 8 (1) (2019) 1538–1549.
[9] K. Gusieva, C.H.J. Davies, J.R. Scully, N. Birbilis, Int. Mater. Rev. 60 (3) (2014) 169–194.
[10] U.M. Chaudry, K. Hamad, J.G. Kim, J. Alloy. Compd. 792 (2019) 652–664.
[11] X. Chen, D.F. Zhang, Y. Zhao, J.K. Feng, B. Jiang, F.S. Pan, Trans. Nonferrous Met. Soc. China 30 (10) (2020) 2650–2657.
[12] W. Cao, S.L. Chen, F. Zhang, K. Wu, Y. Yang, Y.A. Chang, R. Schmid-Fetzer, W.A. Oates, Calphad 33 (2) (2009) 328–342.
[13] Y. Zhang, Y. Liu, S. Liu, H.L. Chen, Q. Chen, S. Wen, Y. Du, J. Mater. Sci. Technol. 62 (2021) 70–82.
[14] X. Xia, A. Sanaty-Zadeh, C. Zhang, A.A. Luo, D.S. Stone, Calphad 60 (2018) 58–67.
[15] B. Liu, Y. Ren, H. Li, M. Jiang, G. Qin, J. Alloy. Compd. 867 (2021) 159070.
[16] W. Zhong, J.C. Zhao, Acta Mater. 201 (2020) 191–208.
[17] B.C. Zhou, S.L. Shang, Y. Wang, Z.K. Liu, Data Brief 5 (2015) 900–912.
[18] J. Zhong, L. Chen, L. Zhang, npj Comput. Mater. 7 (1) (2021).
[19] H. Mehrer, Diffusion in Solid Metals and Alloys, Springer Berlin, 1990.
[20] Z. Zhou, Y. Cui, Q. Wu, G. Xu, L. Zhou, Y. Cui, Calphad 78 (2022).
[21] Y. Zhang, C. Du, Y. Liu, S. Wen, S. Liu, Y. Huang, N. Hort, Y. Du, J. Alloy. Compd. 871 (2021).
[22] W. Zhong, M.S. Hooshmand, M. Ghazisaeidi, W. Windl, J.C. Zhao, Acta Mater. 189 (2020) 214–231.
[23] D.W. Christianson, L. Zhu, M.V. Manuel, Calphad 71 (2020) 101999.
[24] J. Wang, N. Li, C. Wang, J.I. Beltran, J. Llorca, Y. Cui, Calphad 54 (2016) 134–143.
[25] Z.L. Bryan, P. Alieninov, I.S. Berglund, M.V. Manuel, Calphad 48 (2015) 123–130.
[26] W. Zhong, J.C. Zhao, Materialia 7 (2019).
[27] M. Paliwal, I.H. Jung, Calphad 64 (2019) 196–204.
[28] P. Lang, T. Wojcik, E. Povoden-Karadeniz, A. Falahati, E. Kozeschnik, J. Alloy. Compd. 609 (2014) 129–136.
[29] S. Ouyang, G. Yang, C. Chen, T. Bai, H. Qin, C. Wang, L. Zhang, W. Jie, Scr. Mater. 213 (2022).
[30] Q. Tan, Y. Yin, N. Mo, M. Zhang, A. Atrens, Surf. Innov. 7 (2) (2019) 71–92.
[31] S.P. Cashion, N.J. Ricketts, P.C. Hayes, J. Light Met. 2 (2002) 6.
[32] F. Czerwinski, Corros. Sci. 46 (2) (2004) 377–386.
[33] W.D. Callister, D.G. Rethwisch, Materials Science and Engineering: An Introduction (2013).
[34] P.G. Shewmon and F.N. Rhines, *J. Metall.*, **6**, 1954, 1021–1025.
[35] P.G. Shewmon, J. Metall. 8 (1956) 918–922.
[36] J. Combronde, G. Brebec, Acta Metall. 20 (1972).
[37] S. Fujikawa, J. Jpn. Inst. Light Met. 42 (12) (1992) 826–827.
[38] J. Cermak, I. Stloukal, Phys. Status Solidi A 203 (10) (2006) 2386–2392.
[39] S. Brennan, A.P. Warren, K.R. Coffey, N. Kulkarni, P. Todd, M. Kilmov, Y. Sohn, J. Ph. Equilibria Diffus. 33 (2) (2012) 121–125.
[40] N.S. Kulkarni, R.J. Bruce Warmack, B. Radhakrishnan, J.L. Hunter, Y. Sohn, K.R. Coffey, G.E. Murch, I.V. Belova, J. Ph. Equilibria Diffus. 35 (6) (2014) 762–778.
[41] L. Yang, Y. Yuan, J. Liu, T. Chen, A. Tang, F. Pan, Vacuum (2021) 191.
[42] J.C. Zhao, Diffusion Multiple Screening: Phase Diagram Determination and Related Studies, Elsevier, Oxford, 2005.
[43] R. Dong, G. Xu, W.S. Ko, J. Wang, X. Tao, Y. Cui, Calphad 72 (2021).
[44] K. Cheng, H. Xu, B. Ma, J. Zhou, S. Tang, Y. Liu, C. Sun, N. Wang, M. Wang, L. Zhang, Y. Du, J. Alloy. Compd. 810 (2019).
[45] C.C. Kammerer, N.S. Kulkarni, R.J. Warmack, Y.H. Sohn, J. Alloy. Compd. 617 (2014) 968–974.
[46] K.N. Kulkarni, A.A. Luo, J. Ph. Equilibria Diffus. 34 (2) (2013) 104–115.

[47] S. Brennan, K. Bermudez, Y. Sohn, in: Proceedings of the 9th International Conference on Magnesium Alloys and their Applications, 2012.
[48] K. Bermudez, S. Brennan, Y.H. Sohn, Magnes. Technol. (2012) 4.
[49] S. Brennan, K. Bermudez, N.S. Kulkarni, Y. Sohn, Metall. Mater. Trans. A 43 (11) (2012) 4043–4052.
[50] D.J. Hodkin, P.G. Mardon, J. Nucl. Mater. 16 (1965).
[51] L. Yang, Y. Yuan, T. Chen, X. Dai, L. Zhang, D. Li, A. Tang, W. Yi, L. Zhang, F. Pan, Intermetallics 133 (2021) 107171.
[52] Y.F. Ouyang, K. Liu, C.Y. Peng, H.M. Chen, X.M. Tao, Y. Du, Calphad 65 (2019) 204–211.
[53] M. Paliwal, S.K. Das, J. Kim, I.H. Jung, Scr. Mater. 108 (2015) 11–14.
[54] A. Mostafa, M. Medraj, J. Mater. Res. 29 (13) (2014) 1463–1479.
[55] S.K. Das, N. Brodusch, R. Gauvin, I.H. Jung, Scr. Mater. 80 (2014) 41–44.
[56] S.K. Das, I.H. Jung, Mater. Charact. 94 (2014) 86–92.
[57] S.K. Das, Y.B. Kang, T. Ha, I.H. Jung, Acta Mater. 71 (2014) 164–175.
[58] S.K. Das, Y.M. Kim, T.K. Ha, R. Gauvin, I.H. Jung, Metall. Mater. Trans. A 44 (6) (2013) 2539–2547.
[59] S.K. Das, Y.M. Kim, T.K. Ha, I.H. Jung, Calphad 42 (2013) 51–58.
[60] J. Wang, W. Zheng, G. Xu, J. Llorca, Y. Cui, J. Alloy. Compd. 805 (2019) 237–246.
[61] L. Xiao, N. Wang, J. Nucl. Mater. 456 (2015) 389–397.
[62] W. Liu, L. Long, Y. Ma, L. Wu, J. Alloy. Compd. 643 (2015) 34–39.
[63] Y.P. Ren, G.W. Qin, S. Li, Y. Guo, X.L. Shu, L.B. Dong, H.H. Liu, B. Zhang, J. Alloy. Compd. 540 (2012) 210–214.
[64] H.D. Zhao, G.W. Qin, Y.P. Ren, W.L. Pei, D. Chen, Y. Guo, J. Alloy. Compd. 509 (3) (2011) 627–631.
[65] Y. Xu, L.S. Chumbley, G.A. Weigelt, F.C. Laabs, J. Mater. Res. 16 (11) (2011) 3287–3292.
[66] C.C. Kammerer, N.S. Kulkarni, B. Warmack, Y.H. Sohn, J. Ph. Equilibria Diffus. 37 (1) (2016) 65–74.
[67] K. Cheng, J. Sun, H. Xu, J. Wang, C. Zhan, R. Ghomashchi, J. Zhou, S. Tang, L. Zhang, Y. Du, J. Mater. Sci. Technol. 60 (2021) 222–229.
[68] Z. Zhou, Y. Gu, G. Xu, Y. Guo, Y. Cui, Calphad 68 (2020).
[69] X. Zhang, D. Kevorkov, M.O. Pekguleryuz, J. Alloy. Compd. 501 (2) (2010) 366–370.
[70] J. Dai, H. Xiao, B. Jiang, H. Xie, C. Peng, Z. Jiang, Q. Zou, Q. Yang, F. Pan, J. Mater. Sci. Technol. 34 (2) (2018) 291–298.
[71] W. Zhong, J.C. Zhao, Materialia 11 (2020).
[72] W. Zhong, J.C. Zhao, Scr. Mater. 127 (2017) 92–96.
[73] W. Zhong, J.C. Zhao, Metall. Mater. Trans. A 48 (12) (2017) 5778–5782.
[74] L. Boltzmann, Annu. Rev. Phys. Chem. 53 (1894) 6.
[75] Q. Zhang, J.C. Zhao, Intermetallics 34 (2013) 132–141.
[76] F. Sauer, V. Freise, Z. Elektrochem 66 (1962).
[77] L.D. Hall, J. Chem. Phys. 21 (1) (1953) 87–89.
[78] G. Wagner, Acta Metall. 17 (1969) 9.
[79] T. Ahmed, I.V. Belova, A.V. Evteev, E.V. Levchenko, G.E. Murch, J. Ph. Equilibria Diffus. 36 (4) (2015) 366–374.
[80] G. Kresse, J. Furthmüller, Phys. Rev. B 54 (16) (1996) 11169–11186.
[81] J.P. Perdew, A. Ruzsinszky, G.I. Csonka, O.A. Vydrov, G.E. Scuseria, L.A. Constantin, X. Zhou, K. Burke, Phys. Rev. Lett. 100 (13) (2008) 136406.
[82] J.P. Perdew, K. Burke, M. Ernzerhof, Phys. Rev. Lett. 77 (1996).
[83] B.C. Zhou, A Computional Study of the Effects of Alloying Elements on the Thermodynamic and Diffusion Properties of Mg Alloys, The Pennsylvania State University, 2015.
[84] M.S. Hooshmand, W. Zhong, J.C. Zhao, W. Windl, M. Ghazisaeidi, Data Brief 30 (2020) 105381.
[85] R. Agarwal, D.R. Trinkle, Acta Mater. 150 (2018) 339–350.
[86] M.A. Blanco, E. Francisco, V. Luaña, Comput. Phys. Commun. 158 (1) (2004) 57–72.
[87] S.L. Shang, Y. Wang, D. Kim, Z.K. Liu, Comput. Mater. Sci. 47 (4) (2010) 1040–1048.
[88] A.D.L. Claire, J. Nucl. Mater. (1978) 69–70.
[89] D.R. Trinkle, Philos. Mag. 97 (28) (2017) 2514–2563.
[90] G.B. J.Combronde, Acta Metall. 19 (12) (1971) 7.
[91] G. Nandipati, N. Govind, A. Andersen, A. Rohatgi, J. Phys. Condens. Matter. 28 (15) (2016) 155001.
[92] S. Ganeshan, L.G. Hector, Z.K. Liu, Comput. Mater. Sci. 50 (2) (2010) 301–307.
[93] H. Wu, T. Mayeshiba, D. Morgan, Sci. Data 3 (2016) 160054.
[94] B.C. Zhou, S.L. Shang, Y. Wang, Z.K. Liu, Acta Mater. 103 (2016) 573–586.
[95] M. Mantina, Dissertations and Theses, 2008.
[96] M. Mantina, L.Q. Chen, Z.K. Liu, Defect Diffus. Forum 294 (2009) 1–13.
[97] D.S. Gornyj, R.M. Al'tovskij, Fiz. Met. Metalloved. 30 (1) (1970) 85–90.
[98] Y. Xu, L.S. Chumbley, F.C. Laabs, J. Mater. Res. 15 (11) (2000).
[99] K. Lal, V. Levy, Compt. Rend. Ser. C 262 (1966) 107–109 Medium: X; Size: Pages2009-12-15.
[100] S. Ganeshan, L.G. Hector, Z.K. Liu, Acta Mater. 59 (8) (2011) 3214–3228.
[101] V.F. Erko, V.F. Zelenskii, V.S. Krasnorutskii, Fiz. Metal. Metalloved. 22 (1966) Medium: X 2009-12-15.
[102] L.V. Pavlinov, A.M. Gladyshev, V.N. Bykov, Phys. Met. Metallogr. 26 (1968) 53–59.
[103] J. Dai, B. Jiang, J. Zhang, Q. Yang, Z. Jiang, H. Dong, F. Pan, J. Ph. Equilibria Diffus. 36 (6) (2015) 613–619.
[104] I. Stloukal, J. Cermák, Metal (2004) 1–7.
[105] C. Kammerer, N. Kulkarni, R. Warmack, Y. Sohn, Magnes. Technol. (2014) 2014.
[106] V.D. Divya, U. Ramamurty, A. Paul, Philos. Mag. 93 (17) (2013) 2190–2206.
[107] J. Yao, Y.W. Cui, H. Liu, H. Kou, J. Li, L. Zhou, Calphad 32 (3) (2008) 602–607.
[108] H.J. Frost, M.F. Ashby, Deformation-Mechanism Maps: the Plasticity and Creep of Metals and Ceramics, Pergamon Press, 1982 [Oxfordshire].
[109] I. Stloukal, Scr. Mater. 49 (6) (2003) 557–562.
[110] J. Čermák, I. Stloukal, D. Eversheim, Kovove Mater. 44 (2006) 5.
[111] J.O. Andersson, J. Ågren, J. Appl. Phys. 72 (4) (1992) 1350–1355.
[112] W. Sun, C. Zhang, A.D. Klarner, W. Cao, A.A. Luo, Magnesium Technology, The Minerals, Metals & Materials Society, 2015 2015 (Ed.).
[113] J. Zhong, L. Zhang, X. Wu, L. Chen, C. Deng, J. Mater. Sci. Technol. 48 (2020) 163–174.
[114] E. Kozeschnik, J. Svoboda, P. Fratzl, F.D. Fischer, Mater. Sci. Eng. A 385 (1-2) (2004) 157–165.
[115] W. Cao, F. Zhang, S.L. Chen, C. Zhang, Y.A. Chang, JOM 63 (7) (2011) 6.
[116] C. Zhang, W. Cao, S.L. Chen, J. Zhu, F. Zhang, A.A. Luo, R. Schmid-Fetzer, JOM 66 (3) (2014) 389–396.
[117] X. Xia, W. Sun, A.A. Luo, D.S. Stone, Acta Mater. 111 (2016) 335–347.
[118] G.B. Olson, H.J. Jou, J. Jung, J.T. Sebastian, A. Misra, I. Locci, D. Hull, in: Precipitation Model Validation in 3rd Generation Aeroturbine Disc Alloys, The Minerals, Metals & Materials Society, 2008, p. 10.
[119] H.J. Jou, P. Voorhees, G. B.Olson, in: Superalloys 2004, The Minerals, Metals & Materials Society, 2004, p. 10.
[120] K. Wu, Q. Chen, P. Mason, J. Ph. Equilibria Diffus. 39 (5) (2018) 571–583.
[121] W. Wagner, G. Erlhof, in: Praktische Baustatik: Teil 2, Vieweg+Teubner Verlag, Wiesbaden, 1991, pp. 213–282.
[122] J.S. Langer, A.J. Schwartz, Phys. Rev. A 21 (3) (1980) 948–958.
[123] R. Wagner, R. Kampmann, P.W. Voorhees, Phase Transformations in Materials, Wiley, 1991 -VCH.
[124] Q. Chen, J. Jeppsson, J. Ågren, Acta Mater. 56 (8) (2008) 1890–1896.
[125] S. Celotto, Acta Mater. 48 (2000) 13.
[126] C.L. Mendis, C.J. Bettles, M.A. Gibson, S. Gorsse, C.R. Hutchinson, Philos. Mag. Lett. 86 (7) (2006) 443–456.
[127] S Celotto, T.J. Bastow, Acta Mater. 49 (1) (2001) 12.
[128] B.D. Lee, E.J. Kim, U.H. Baek, J.W. Han, Met. Mater. Int. 19 (2) (2013) 135–145.

[129] W.T. Sun, X.G. Qiao, M.Y. Zheng, C. Xu, S. Kamado, X.J. Zhao, H.W. Chen, N. Gao, M.J. Starink, Acta Mater. 151 (2018) 260–270.
[130] C. Liu, X. Chen, D. Tolnai, Y. Hu, W. Zhang, Y. Zhang and F. Pan, *J. Mater. Sci. Technol.*, **144**, 2023, 70–80.
[131] C.R. Hutchinson, J.F. Nie, S. Gorsse, Metall. Mater. Trans. A 36A (2005).
[132] C.H. Cáceres, J.R. Griffiths, A.R. Pakdel, C.J. Davidson, Mater. Sci. Eng. A 402 (1-2) (2005) 258–268.
[133] Z.M. Li, A.A. Luo, Q.G. Wang, L.M. Peng, P.H. Fu, G.H. Wu, Mater. Sci. Eng. A 564 (2013) 450–460.
[134] P.H. Fu, L.M. Peng, H.Y. Jiang, J.W. Chang, C.Q. Zhai, Mater. Sci. Eng. A 486 (1-2) (2008) 183–192.
[135] G. Zhao, Z. Zhang, Y. Zhang, H. Peng, Z. Yang, H. Nagaumi, X. Yang, Mater. Sci. Eng. A 834 (2022).
[136] H. Oikawa, Y. Iijima, Diffusion behavior of creep-resistant steels, Creep-Resistant Steels, Woodhead Publishing Series in Metals and Surface Engineering, 2008, pp. 241–264, doi:10.1533/9781845694012.2.241.
[137] H. Front, M. Ashby, in: Deformation Mechanisms and Deformation-Mechanism Maps, Pergamon Press, 1982, p. 44.
[138] K.R. Athul, U.T.S. Pillai, A. Srinivasan, B.C. Pai, Adv. Eng. Mater. 18 (5) (2016) 770–794.
[139] R.L. Coble, J. Appl. Phys. 34 (6) (1963) 1679–1682.
[140] M. Pekguleryuz, M. Celikin, Int. Mater. Rev. 55 (4) (2013) 197–217.
[141] H. Qin, G. Yang, L. Zhang, S. Ouyang, C. Wang, W. Jie, Phys. Status Solidi 218 (6) (2021).
[142] N. Mo, Q. Tan, M. Bermingham, Y. Huang, H. Dieringa, N. Hort, M.X. Zhang, Mater. Des. 155 (2018) 422–442.
[143] Y. Zhang, Z. Liu, S. Pang, T. Meng, Y. Zhi, Y. Xu, L. Xiao, R. Li, Mater. Sci. Eng. A (2021) 805.
[144] L. Zhang, M. Wu, C. Xu, S. Guo, Z.L. Ning, F.Y. Cao, Y.J. Huang, J.F. Sun, J. Yi, Mater. Sci. Eng. A 827 (2021).
[145] S. Ouyang, G. Yang, H. Qin, C. Wang, S. Luo, W. Jie, J. Magnes. Alloy. (2021).
[146] J. Wang, G. Xu, X. Zeng, J. Llorca, Y. Cui, Mater. Des. 197 (2021).
[147] R. Mahmudi, S. Moeendarbari, Mater. Sci. Eng. A 566 (2013) 30–39.
[148] S. Rashno, B. Nami, S.M. Miresmaeili, Mater. Des. 60 (2014) 289–294.
[149] B. Nami, S. Rashno, S.M. Miresmaeili, J. Alloy. Compd. 639 (2015) 308–314.
[150] B. Nami, S.M. Miresmaeili, F. Jamshidi, I. Khoubrou, Trans. Nonferrous Met. Soc. China 29 (10) (2019) 2056–2065.
[151] A.K.S. Bankoti, A.K. Mondal, H. Dieringa, B.C. Ray, S. Kumar, Mater. Sci. Eng. A 673 (2016) 332–345.
[152] S.M. Ashrafizadeh, R. Mahmudi, A.R. Geranmayeh, Mater. Sci. Eng. A 790 (2020).
[153] H.K. Kim, J. Mater. Sci. 39 (2004) 3.
[154] R. Alizadeh, R. Mahmudi, T.G. Langdon, Mater. Sci. Eng. A 564 (2013) 423–430.